1-28-2011

A size-dependent nanoscale metal–insulator transition in random materials

Albert B.K. Chen
University of Pennsylvania, albertbk@seas.upenn.edu

Soo Gil Kim
University of Pennsylvania

Yudi Wang
University of Pennsylvania, wangyudi@seas.upenn.edu

Wei-Shao Tung
University of Pennsylvania, tungwei@seas.upenn.edu

I-Wei Chen
University of Pennsylvania, iweichen@seas.upenn.edu

A size-dependent nanoscale metal–insulator transition in random materials

Abstract
Insulators and conductors with periodic structures can be readily distinguished, because they have different band structures, but the differences between insulators and conductors with random structures are more subtle. In 1958, Anderson provided a straightforward criterion for distinguishing between random insulators and conductors, based on the 'diffusion' distance ζ for electrons at 0 K (ref. 3). Insulators have a finite ζ, but conductors have an infinite ζ. Aided by a scaling argument, this concept can explain many phenomena in disordered electronic systems, such as the fact that the electrical resistivity of 'dirty' metals always increases as the temperature approaches 0 K (refs 4–6). Further verification for this model has come from experiments that measure how the properties of macroscopic samples vary with changes in temperature, pressure, impurity concentration and applied magnetic field, but, surprisingly, there have been no attempts to engineer a metal–insulator transition by making the sample size less than or more thanζ. Here, we report such an engineered transition using six different thin-film systems: two are glasses that contain dispersed platinum atoms, and four are single crystals of perovskite that contain minor conducting components. With a sample size comparable to ζ, transitions can be triggered by using an electric field or ultraviolet radiation to tune ζ through the injection and extraction of electrons. It would seem possible to take advantage of this nanometallicity in applications.

Disciplines
Engineering | Materials Science and Engineering

Comments
Postprint version.

Suggested Citation:
Chen, A.B.K., Kim, S.G., Wang, Y. Tung, W. and Chen, I. (2011). A size-dependent nanoscale metal–insulator transition in random materials *Nature Nanotechnology*, Vol. 6. pp. 237-241.

Publisher URL: http://dx.doi.org/10.1038/nnano.2011.21

nature nanotechnology

LETTERS

PUBLISHED ONLINE: XX XX 2011 | DOI: 10.1038/NNANO.2011.21

A size-dependent nanoscale metal–insulator transition in random materials

Albert B. K. Chen†, Soo Gil Kim†, Yudi Wang†, Wei-Shao Tung and I-Wei Chen*

Insulators and conductors with periodic structures can be readily distinguished, because they have different band structures, but the differences between insulators and conductors with random structures are more subtle[1,2]. In 1958, Anderson provided a straightforward criterion for distinguishing between random insulators and conductors, based on the 'diffusion' distance ζ for electrons at 0 K (ref. 3). Insulators have a finite ζ, but conductors have an infinite ζ. Aided by a scaling argument, this concept can explain many phenomena in disordered electronic systems, such as the fact that the electrical resistivity of 'dirty' metals always increases as the temperature approaches 0 K (refs 4–6). Further verification for this model has come from experiments that measure how the properties of macroscopic samples vary with changes in temperature, pressure, impurity concentration and applied magnetic field[4,5], but, surprisingly, there have been no attempts to engineer a metal–insulator transition by making the sample size less than or more than ζ. Here, we report such an engineered transition using six different thin-film systems: two are glasses that contain dispersed platinum atoms, and four are single crystals of perovskite that contain minor conducting components. With a sample size comparable to ζ, transitions can be triggered by using an electric field or ultraviolet radiation to tune ζ through the injection and extraction of electrons. It would seem possible to take advantage of this nanometallicity in applications.

We studied nominally insulating thin films that had a random composition (perovskite crystals) or an outright amorphous structure (glasses) and included minor conducting components. To unambiguously distinguish a size-triggered metal–insulator transition (MIT) from conventional percolation[6], in which conductivity persists over a macroscopic length scale, we focused on compositions with a conducting fraction f well below the bulk percolation limits (these are listed for several systems in Table 1). Aiming at a nanoscale ζ, we probed ζ in films of various nanoscale thickness δ: films with $\delta \ll \zeta$ are metallic across the thickness, films with $\delta \gg \zeta$ are insulating. We also examined films with $\delta \approx \zeta$ to attempt an externally stimulated MIT. All the films studied had macroscopic lateral sizes, so laterally they were insulating.

Our first example was amorphous SiO_2 doped with Pt atoms finely dispersed at the scale of <0.5 nm (the transmission electron micrograph and corresponding electron diffraction are shown in the insets of Fig. 1a,b, respectively). The lateral percolation limit was $f \approx 0.38$ (molar fraction of Pt in SiO_2:Pt); above this the sheet resistance (per four-point probe) decreased with decreasing temperature T, and below it, the opposite held (Supplementary Fig. S1). At $f \geq 0.33$, the UV reflectivity shows a peak at 270 nm (Fig. 1), which is the plasmon resonance of metallic Pt nanoparticles in SiO_2; this signature resonance is also commonly used to characterize dispersed nanoparticles of Au and Ag of dilute concentrations[7]. There is no such peak at $f = 0.2$, suggesting the absence of metallic clusters. Despite the lack of metallic clusters, evidence for free carriers at $f = 0.2$ appeared in the long-wavelength (>15 μm) optical data under the characteristic SiO_2 vibration peak (Fig. 1b). At increasing wavelengths, there is an increasing reflectivity background that can be fitted by Drude's formula for dissipative conducting electrons[8]. The fitted plasma energy is ~0.068 eV, corresponding to a carrier (assuming free electron) concentration of 8.4×10^{16} cm^{-3}. The concentration increased to 1.47×10^{17} cm^{-3} at $f = 0.29$. Therefore, in these SiO_2:Pt glasses, we have found a material that is macroscopically insulating, but (infrared) optically conducting, which fits Anderson's picture of a random insulator with a finite ζ.

We expect a $\delta \ll \zeta$ film to be an ohmic conductor and a $\delta \gg \zeta$ one to be a non-ohmic insulator, so resistance–voltage testing across the film thickness (Fig. 2a) offers a way to determine ζ. For $f = 0.2$, the virgin film was ohmic up to $\delta = 16$ nm. At 21 nm, it was non-ohmic with a high resistance. Here, a positive voltage V refers to having a current I flowing across a test cell from top to bottom, with a resistance $R = V/I$. This would suggest 16 nm < ζ < 21 nm. However, we also found that films with thicknesses from 7 nm to 16 nm underwent a voltage-induced MIT: a R–V hysteresis between two resistance states (HR, high resistance; LR, low resistance) switching at a certain sharp 'set' voltage V_{set} from LR to HR, then reversing at several step-like 'reset' voltages V_{reset}. The HR state of the 16 nm film (broken curve in Fig. 2a) was particularly precarious, varying from run to run and from cell to cell. In contrast, the thicker film (21 nm) in Fig. 2a (for $f = 0.2$) had a stable high resistance that did not switch, whereas a film of a similar thickness (20 nm) but higher f had an ohmic low resistance in the virgin state, then switched at about the same voltage (Fig. 2c). These results are summarized in the δ–f map in Fig. 2b, which delineates a relatively wide window for voltage-induced MIT. Such data allow us to define

Table 1 | Nanometallic thin films with $\zeta \approx 20$ nm.

Solid solutions	f_c (mol%)	V_{set} (eV)	Predicted FNT barrier (eV)	$f_{percolation}$ (mol%)
CZO-SRO	5.5	2.2	2.5	75
LAO-SRO	11	2.2	2.5	86
CZO-LNO	25	2.2	2.5	-
LAO-LNO	12	2.2	2.5	-
SiO_2-Pt	29	4.2	4.1	38
$SiN_{4/3}$-Pt	25	3.0	2.9	38

For Si_3N_4:Pt, $\zeta \approx 25$ nm. Values of f_c (in mol% of conductor) are insensitive to electrode material (Pt, Au, SRO, Mo, Ag, and Ta, in the order of decreasing work function) and substrate orientation (001, 011 and 111 STO for perovskites and 100 and 110 Si for amorphous solutions of SiO_2:Pt and Si_3N_4:Pt.) Values of V_{set} (top electrode, Pt; bottom electrode, SRO) are in agreement with the predicted Fowler–Nordheim tunnelling barrier from the highest occupied state of the less noble electrode (SRO) to the lowest unoccupied state of the insulator. Electron tunnelling at V_{set} is directed from the less noble electrode to the more noble electrode (see Supplementary Figs S2, S3 and S7 and Table S1 for details). The bulk percolation limits are estimates from the macroscopic MIT data summarized in Supplementary Section A.

Department of Materials Science & Engineering, University of Pennsylvania, Philadelphia, Pennsylvania 19104, USA; †These authors contributed equally to this work. *e-mail: iweichen@seas.upenn.edu

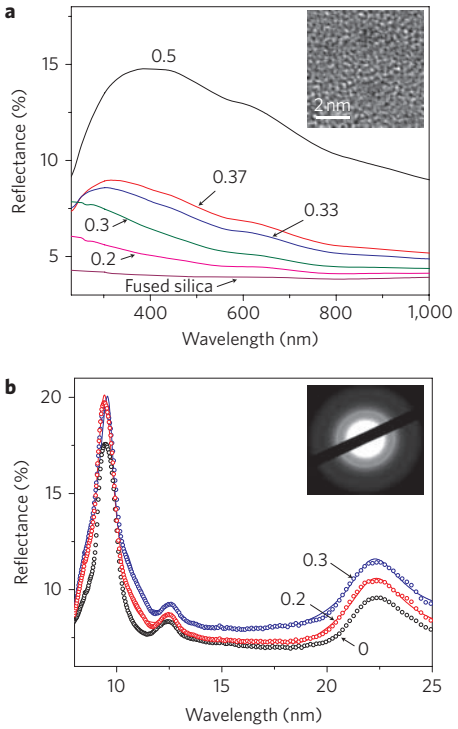

Figure 1 | Optical evidence of metallic clusters and free carriers. a, UV reflectivity of 40 nm SiO_2:Pt films; the peak at 270 nm characteristic of metallic Pt nanoparticles is completely absent at $f = 0.2$. Inset: transmission electron micrograph of 12 nm SiO_2:0.2 Pt film with a worm-like random structure without apparent segregation. **b**, Infrared reflectivity (200 nm films) featuring, at $f = 0$, only the vibrational peaks (at 9.5, 12.5, 22.5 nm) of SiO_2, and at $f > 0$ the same peaks plus a background due to dissipative conducting electrons. Electron contribution increases with wavelength, causing an increase of peak intensity at 22.5 nm with Pt content, in agreement with the Drude model fitting the data (shown as solid curves for $f = 0.2$ and 0.3). Inset: electron diffraction pattern of 12 nm SiO_2:0.2 Pt film with a diffuse ring typical of amorphous material[27].

a statistically more meaningful ζ as the mid-point in the window; ζ gradually increases with f, and suddenly diverges as f approaches the bulk percolation limit.

Remarkably, regardless of their locations in the map, all the switchable films had a V_{set} that was independent of f and δ (Fig. 2b, inset). This indicates that switching is not field-dependent, instead having an energetic origin. It is also consistent with its temperature (T) dependence, or lack thereof; at lower T, the hysteresis loop (Fig. 2c) expanded vertically but V_{set} remained unchanged. This argues against a thermally activated switching mechanism, such as ionic/atomic migration or electron hopping. In the literature, many insulators have been reported to undergo reversible resistance switching triggered by the huge electric field across a thin film, which either motivated atomic/ionic motion over a distance of several unit cells to form/break conducting filaments or charged barrier layers, or enabled redox reactions, especially at electrode interfaces[9–16]. Recently[15,16], UV irradiation was found to lower the resistance of switchable TiO_2/molecular junctions that underwent redox reactions (at the external surface), and likewise of Cu_xO films that contained conducting filaments that were subsequently broken. This implies that UV irradiation can enable electronic switching via the redox mechanism if excess electrons and holes are immediately transported away; otherwise, they will reverse/negate the redox reactions. In our film, nanometallicity naturally provided this function. This means that the entire film may be able to undergo UV-enabled electronic switching by mechanisms that must be accompanied by draining of excess electrons or holes. Indeed, without applying a voltage, we found UV irradiation was able to revive a 'dead' cell stuck at the HR after repeated switching (Fig. 3a). Clearly, there was no long-range atomic/ionic motion here to repair the 'fatigue' damage. (Electron trapping/detrapping could be one switching mechanism, which can operate under both voltage and UV stimulation.)

Parallel observations of nanometallic MIT were made in other random materials. One was a Si_3N_4 glass similarly doped with Pt, the other adopted a lattice construct that was perfectly regular but randomized by atomic mixing—a perovskite solid solution made into an epitaxial thin film to avoid line and planar defects that might have provided electrical shorts[17,18]. These solid solutions were hosted by either $LaAlO_3$ (LAO) or $CaZrO_3$ (CZO), two excellent insulators, and doped with a small amount of $LaNiO_3$ (LNO) or $SrRuO_3$ (SRO), two well-known electronic conductors. Although mismatches between cations of different valences and sizes occupying the so-called A site ($Sr^{2+} > La^{3+} > Ca^{2+}$) and the B site ($Zr^{4+} > Ru^{4+} > Ni^{3+} > Al^{3+}$) could have motivated cation ordering or segregation in these solid solutions, we avoided it by lowering the deposition temperature. Therefore, even at a relatively high fraction such as $f = 0.25$ in a 3:1 mixture of CZO and LNO, the high-resolution cross-sectional image of Fig. 4 and its Fourier transform (Fig. 4, inset) revealed only intense diffuse scattering (expected for a concentrated random solid solution) and no evidence of ordering or phase separation. Their MIT could all be triggered by varying δ or

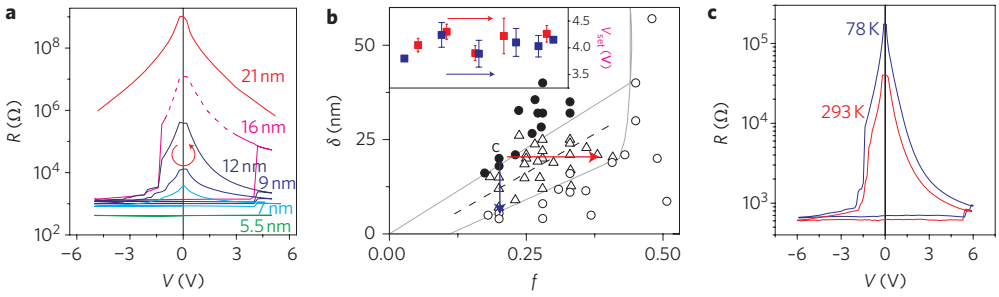

Figure 2 | *R–V* dependence on thickness, composition and temperature. a, Cycle from 0 V, to (-) V, to (+) V, to (-) V, to 0 V traces a *R–V* loop for SiO_2:0.2 Pt of various thickness. These are 'first loops'; that is, samples were not subject to any previous electrical stimulus/forming. When $\delta \approx \zeta$, the hysteresis loop provides non-volatile memory. Top electrode, Pt; bottom electrode, Mo. **b**, δ–f map for SiO_2:f Pt delineating boundaries for conductors (open circles) and insulators (filled circles) separated by switchable films (triangles), abruptly rising at $f \approx 0.4$ near the bulk percolation limit. Top electrode, Pt; bottom electrode, $SrRuO_3$ and Mo (same results). The bisector (broken line) between the boundaries is taken as ζ. Inset: f–δ independent V_{set} for samples along the horizontal red arrow (same δ, increasing f, as red squares) and vertical blue arrow (same f, decreasing δ, as blue squares). **c**, *R–V* loops at two temperatures for 20 nm SiO_2:0.25 Pt. Top electrode, Pt; bottom electrode, Mo. Note that f in **c** is higher than in **a**.

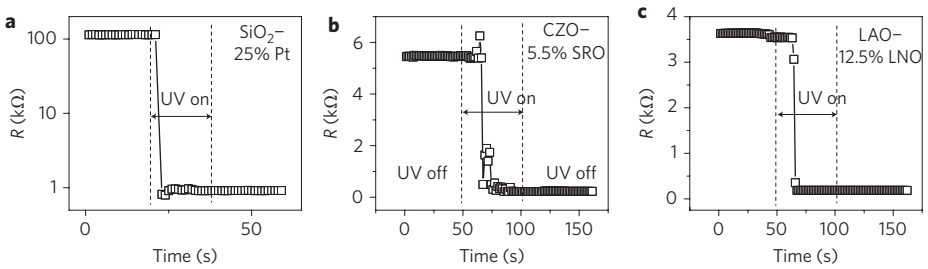

Figure 3 | UV-triggered HR-to-LR transitions. a, HR of a fatigue-damaged cell promptly decreases when UV is turned on at room temperature. (The low resistance stayed permanently after the light was turned off. The outcome was identical, whether the cell was shorted to the ground or under a small positive/negative bias voltage.) 20 nm SiO_2:0.25 Pt; top electrode, Pt; bottom electrode, Mo. **b**,**c**, Further examples of UV-triggered HR-to-LR transitions in $CaZrO_3$:0.055 $SrRuO_3$ (**b**) and $LaAlO_3$:0.125 $LaNiO_3$ (**c**) films. (For other examples see Supplementary Fig. S4.).

the voltage (Supplementary Fig. S2, S3), and their HR-to-LR transition could be rendered by UV irradiation without application of a voltage (Fig. 3b,c). δ–f maps similar to the one in Fig. 2b were also observed, as was a δ–f–T independent V_{set}. Moreover, despite the large differences in structure, chemistry and f (see Table 1), the traces for their hysteretic loops (Supplementary Fig. S2, S3) all proceeded in the same, anticlockwise manner as in Fig. 2a, provided the top electrode (for example, Pt) had a higher work function than the bottom electrode (for example, SRO). All these observations, common to every nanometallic random material studied here, are supportive of an electronic mechanism.

Despite their similarity, different random materials did have different $\zeta(f)$ dependence. Table 1 lists the requisite f_c to render metallicity with $\zeta \approx 20$ nm. The perovskite data are particularly interesting. First, nanometallicity at low f_c values is itself remarkable, because the bulk percolation limit in these materials is typically at $f > 0.7$ (Table 1): a conducting perovskite rapidly loses bulk metallicity with a very modest addition of apparently any insulating perovskite[19]. The very low f_c of perovskites thus firmly rejects the notion that nanometallicity is due to percolation between metallic nanoparticles. Second, the f_c of perovskites appears to be correlated to the electron wave function of the cation (more extended for Ru-4d than for Ni-3d in the conducting component) and their valence variation ($\Delta Z = 0$ for Ru^{4+}/Zr^{4+} and Ni^{3+}/Al^{3+}, but not other pairs of B-site cations). The smallest f_c is required for CZO:SRO (more extended, $\Delta Z = 0$), more for LAO:SRO (more extended, $\Delta Z \neq 0$) and LAO:LNO (less extended, $\Delta Z = 0$), and most for CZO:LNO (less extended, $\Delta Z \neq 0$). This correlation may be used to guide perovskite formulation in engineering nanometallicity in the absence of a detailed knowledge of electronic structure in random materials. Compared to perovskites, the amorphous SiO_2:Pt and Si_3N_4:Pt have more extended Pt-5d electrons but also considerably greater structural and charge disorders, so their f_c is higher and closer to the bulk percolation limit.

We now compare the LR and HR states with the conventional metallic and insulating states. In Fig. 2c, the rapid decrease of the HR with T is consistent with an insulating state, but the decrease of LR with T is too modest for a typical insulator. (Later, in Fig. 5b, we will find that LR can also increase with T.) Using SRO as the bottom electrode, we show in Supplementary Fig. S6 that the LR was mainly due to the spreading resistance of the bottom electrode: its T dependence mirrored that of SRO, a ferromagnetic metal, featuring a spin-fluctuation-scattering kink at the Curie temperature (160 K)[20]. Importantly, even with the spreading resistance contribution, the LR remained finite and small as T approached 0 K. So, LR must be metal-like and cannot be related to electron hopping between impurity states/bands, for which diminishing thermal activation would have caused a divergent resistance toward 0 K (ref. 6). A metallic LR is also consistent with its ohmic $R(V)$ behaviour, in contrast to the non-ohmic HR.

Because the HR contains only a small contribution from the spreading resistance, we will use it to illustrate some features of nanometallicity. First, the HR does not conform to the Ohm's law of macroscopic resistors. Instead, it follows $R \approx \exp(\delta/a)$, with $a \approx 1.2$ nm being another localization length (Fig. 5a), which is the expected length dependence in the localization regime[4–6]. Therefore, a drastic shortening of ζ to some new localization length commensurate with a occurred at V_{set}, thus triggering the MIT. Physically, we suggest that the transition could be due to the injection of electrons, which are trapped at sites near the original conducting pathways; they then erect Coulomb repulsions that 'choke off' further electron passage along the nanometallic pathway. Assuming electron trapping occurs by Fowler–Nordheim tunnelling (FNT)[21] from the nanometallic path to a trap site, through a barrier that is the gap between the highest occupied state of the conductor and the lowest unoccupied state of the insulator, we estimated the required transition voltage as shown in Table 1. This compares well with the observed V_{set}.

Under a reverse bias, successive detrapping through the same tunnelling barrier typically leaves behind a series of intermediate states. One such set is shown in Fig. 5b (inset) and interrogated using their small signal I–V–T curves ($\pm$0.2 V). As shown Fig. 5b, their resistances all saturated at low T. (Note also the LR increase with T in the bottom curve.) So, again, electron conduction in these states was not thermally activated at sufficiently low temperatures, despite the negative slope of $R(T)$. These characteristics are reminiscent of 'bad' metals and can be quantitatively fitted (curves in Fig. 5b) using Sheng's model of fluctuation-induced

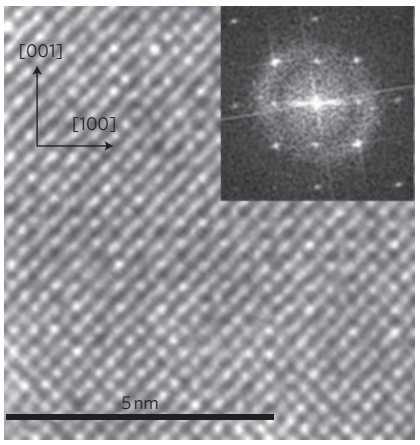

Figure 4 | Random perovskite solid solution. Cross-sectional high-resolution TEM image along the [010] direction of a 3:1 mixture of $CaZrO_3$ and $LaNiO_3$ film (30 nm) on a 100 $SrTiO_3$ substrate with a 30 nm buffer of $SrRuO_3$. Inset: fast Fourier transform of the same region.

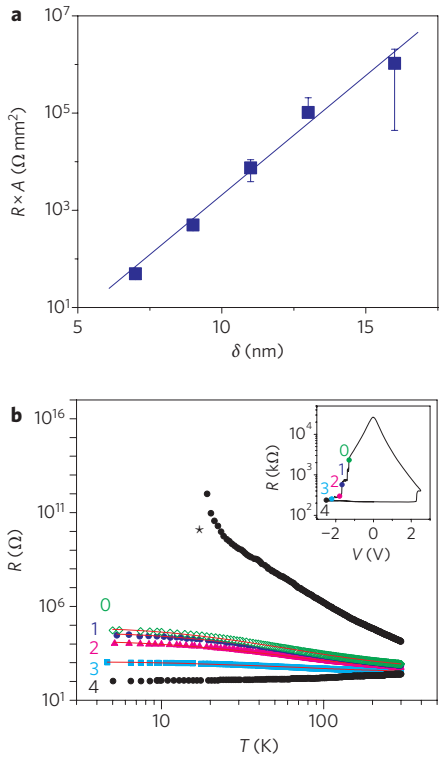

Figure 5 | *R*–δ and *R*–*T* dependencies. a, HR, multiplied by cell area *A*, increases exponentially with film thickness. SiO_2:0.25 Pt; top electrode, Pt; bottom electrode, Mo. **b**, Logarithmic temperature dependence of resistance of the LR state (4) and four intermediate states (0–3) shown in the inset. Also shown are data (*) from another sample with a more resistive HR. Curves 0–3 are model fit using FIT: tunnelling along a metallic channel with one gap of spacing ~0.4–1.2 nm and effective gap capacitor area ~(0.2 nm)^2–(0.8 nm)^2. $LaAlO_3$:0.13 $LaNiO_3$; top electrode, Pt; bottom electrode, $SrRuO_3$.

tunnelling (FIT)[22]. By allowing only elastic electron tunnelling (that is, no thermal activation) between metallic junctions, which are subject to a small junction voltage fluctuation (the Johnson noise) of the order of $(kT/C_{\text{junction}})^{1/2}$, the model predicts a gradual decrease of R with T that is absent in the models for conventional metals. The fitted C_{junction} from Fig. 5b gives the junction geometry: as R decreases with further resetting, the junction gap narrows, signalling that the choked nanometallic path gradually recovers. Such choked nanometallic paths are reminiscent of broken metallic filaments in conventional resistance memories[9–16], although they can be electronically cleared by electron detrapping without atomic/ionic motion. Finally, with more electrons trapped and the nanometallic paths heavily choked, we also observed higher HR values with an insulator-like steep T dependence (one example is marked by * in Fig. 5b). The intermediate and HR states therefore broadly encompass a spectrum of behaviour from bad metals to insulators, depending on the population of trapped electrons and film thickness. Further analysis is provided in Supplementary Fig. S8, which draws an analogy to other bad metals such as conducting polymers[23].

The nanometallicity described here for random materials has a tunable carrier density and localization length ζ. With conducting polymers as an outstanding example[23], we suggest that nanometallicity could be engineered by intimate mixing, at the atomic level, of other conducting and insulating components, which may be crystalline or amorphous, including organic, biological and synthetic hybrid materials. These materials may have unusual, advantageous device characteristics. For example, by slightly reducing their thickness, cells with the exponential $R(\delta)$ dependence can lower the resistance by orders of magnitude to counter the resistance increase due to smaller cell areas. These new materials could also have disparate properties that are otherwise incompatible in conventional materials. Combining length-dependent (and anisotropic if sizes are disparate in different directions) nanometallicity with low thermal conductivity (for example, of SiO_2) and high permittivity (for example, of HfO_2), properties that are of special interest to certain nanostructures[24–26] could be especially intriguing.

Methods

Amorphous SiO_2:Pt and Si_3N_4:Pt films were deposited by radiofrequency co-sputtering using targets of Pt, SiO_2 and Si_3N_4 onto unheated single-crystal Si substrates (110 and 100 orientations) with a pre-deposited polycrystalline SRO electrode. Epitaxial perovskite films were grown on (001) $SrTiO_3$ single-crystal substrates using pulsed laser ablation, with a SRO bottom electrode, at various temperatures. Substrates of (011) and (111) $SrTiO_3$ were also used to vary the growth strain and verify the generality of the observations. Top electrodes were deposited by sputtering (Pt, Mo, Ta) or thermal evaporation (Au, Ag) through a shadow mask with various openings (typically 80 μm in diameter) to define test cells. For SiO_2:Pt, Pt, Mo and Ta were also used as bottom electrodes. The high-resolution cross-sectional images of perovskites were taken with a JEOL 2010 LaB_6 transmission electron microscope operating at 200 kV. The plan-view transmission electron micrographs and diffraction of SiO_2:Pt showing its amorphous structure[27] were taken using films sputter-deposited onto carbon-coated microscopy (copper) grids. Optical reflectivity and transmittance were collected using SiO_2:Pt films deposited onto either fused silica substrates for UV-Vis measurements (Cary 5000 spectrometer from Varian) or KBr substrates for IR measurements (Nicolet 8700 FTIR from Thermo Scientific.) Impedance (d.c. and a.c.) was measured in air using a probe station, and also for UV irradiation (continuous energy of ~2.8–4.1 eV) experiments. Additional measurements (including four-point probing of sheet resistance) were conducted in various cryostats, in vacuum, using lithographically or shadow-mask defined cells of various sizes. In fitting the reflectivity data of Fig. 1b, the free electron contribution to reflectivity of Fig. 1b was fitted using Drude's formula for dielectric constant, $\varepsilon = 1 - \omega_p^2/\omega(\omega + i/\tau)$, to find the plasma frequency ω_p and carrier concentration ($\propto \omega_p^2$). In fitting the data of Fig. 5b, Sheng's equation for tunnelling conductance, $G = 1/R = G_o \exp(-T_1/(T + T_0))$, was used to find T_1 and T_0, from which the geometric parameters of the nanojunctions were obtained. Further details of the methods and the material characterization are provided in the following sections.

Received 24 September 2010; accepted 28 January 2011; published online XX XX 2011

References

1. Mott, N. F. & Davis, E. *Electronic Processes in Non-Crystalline Materials* 2nd edn (Clarendon Press, 1979).
2. Mott, N. F. Electrons in disordered structures. *Adv. Phys.* **16,** 49–144 (1967).
3. Anderson, P. W. Absence of diffusion in certain random lattices. *Phys. Rev.* **109,** 1492–1507 (1958).
4. Dynes, R. C. & Lee, P. A. Localization, interactions, and the metal–insulator transition. *Science* **233,** 355–360 (1984).
5. Lee, P. A. & Ramakrishnan, T. V. Disordered electronic systems. *Rev. Mod. Phys.* **57,** 287–337 (1985).
6. Shklovskii, B. I. & Efros, A. L. *Electronic Properties of Doped Semiconductors* (Springer-Verlag, 1984).
7. Ghosh, S. K. & Pal, T. Interparticle coupling effect on the surface plasmon resonance of gold nanoparticles: from theory to applications. *Chem. Rev.* **107,** 4797–4862 (2007).
8. Gravais, F. Optical conductivity of oxides. *Mater. Sci. Eng.* **R39,** 29–92 (2002).
9. Waser, R., Dittmann, R., Staikov, G. & Szot, K. Redox-based resistive switching memories—nanoionic mechanisms, prospects, and challenges. *Adv. Mater.* **21,** 1632–2663 (2009).
10. Szot, K., Speier, W., Bihlmayer, G. & Waser, R. Switching the electrical resistance of individual dislocations in single-crystalline $SrTiO_3$. *Nature Mater.* **5,** 312–320 (2006).
11. Snider, G. S., Stewart, D. R. & Williams, R. S. The missing memristor found. *Nature* **431,** 80–83 (2008).
12. Rossel, C., Meijer, G. I., Bremaud, D. & Widmer, D. Electrical current distribution across a metal–insulator–metal structure during bistable switching. *J. Appl. Phys.* **90,** 2892–2898 (2001).
13. Sawa, A., Fujii, T., Kawasaki, M. & Tokura, Y. Hysteretic current–voltage characteristics and resistance switching at a rectifying $Ti/Pr_{0.7}Ca_{0.3}MnO_3$ interface. *Appl. Phys. Lett.* **85,** 4073–4075 (2004).
14. Kwon, D-H. *et al.* Atomic structure of conducting nanofilaments in TiO_2 resistive switching memory. *Nature Nanotech.* **5,** 148–153 (2010).

15. Wu, J. & McCreery, R. L. Solid-state electrochemistry in molecule/TiO_2 molecular heterojunctions as the basis of the TiO_2 'memristor'. *J. Electrochem. Soc.* **156,** P29–P37 (2009).
16. Liu, C-Y. & Hsu, J-M. Effect of ultraviolet illumination on resistive switching properties of Cu_xO thin film. *Jpn J. Appl. Phys.* **49,** 084202 (2010).
17. Kim, S. G., Wang, Y-D. & Chen, I-W. Strain relaxation in buried $SrRuO_3$ layer in $(Ca_{1-x}Sr_x)(Zr_{1-x}Ru_x)O_3/SrRuO_3/SrTiO_3$ system. *Appl. Phys. Lett.* **89,** 031905 (2006).
18. Wang, Y-D., Kim, S. G. & Chen, I-W. Strain relaxation in tensile and compressive oxide thin films, *Acta Materialia* **56,** 5312–5321 (2008).
19. Mamchik, A. & Chen, I-W. Magnetic impurities in conducting oxides: I. $(Sr_{1-x}La_x)(Ru_{1-x}Fe_x)O_3$ system. *Phys. Rev. B* **70,** 104409 (2004).
20. Allen, P. B. *et al.* Transport properties, thermodynamic properties, and electronic structure of $SrRuO_3$. *Phys. Rev. B* **53,** 4393–4398 (1996).
21. Lenzling, M. & Snow, E-H. Fowler–Nordheim tunneling into thermally grown SiO_2. *J. Appl. Phys.* **40,** 278–283 (1969).
22. Sheng, P. Fluctuation-induced tunneling conduction in disordered materials. *Phys. Rev. B* **21,** 2180–2195 (1980).
23. Menon, R., Yoon, C. O., Moses, D., Heeger, A. J. & Cao, Y. Transport in polyaniline near the critical regime of the metal–insulator transition. *Phys. Rev. B* **48,** 17685–17694 (1993).
24. Ohta, H. *et al.* Giant thermoelectric Seebeck coefficient of two-dimensional electron gas in $SrTiO_3$. *Nature Mater.* **6,** 129–134 (2007).
25. Ozbay, E. Merging photonics and electrons at nanoscale dimensions. *Science* **311,** 189–193 (2006).
26. Engheta, N. Circuits with light at nanoscales: optical nanocircuits inspired by metamaterials. *Science* **317,** 1698–1702 (2007).
27. Bagley, B. G. & Turnbull, D. The preparation and crystallization behaviour of amorphous nickel–phosphorus thin films. *Acta Metallurgica* **18,** 857–862 (1970).

Acknowledgements

This work was supported by the National Science Foundation (grant nos DMR-05-20020, 07-05054 and 09-07523). For the TEM analysis, we are grateful to K.C. Hsieh and Y. Lu at the Frederick Seitz Materials Research Laboratory (University of Illinois), partially supported by the US Department of Energy (grants DE-FG02-07ER46453 and DE-FG02-07ER46471).

Author contributions

I-W.C. conceived and designed the experiments and wrote the paper. A.B.C. performed the SiO_2:Pt and SiN:Pt experiments. S.G.K. and Y.D.W. performed the perovskite experiments. W.S.T. performed the optical experiments. All authors analysed the data, discussed the results and commented on the manuscript.

Additional information

The authors declare no competing financial interests. Supplementary information accompanies this paper at www.nature.com/naturenanotechnology. Reprints and permission information is available online at http://npg.nature.com/reprintsandpermissions/. Correspondence and requests for materials should be addressed to I.W.C.

Publisher: Nature

Journal: Nature Nanotechnology

Article number nnano.2011.21

Author (s): Albert B. K. Chen *et al*.

Title of paper: A size-dependent nanoscale metal–insulator transition in random materials

Query no.	Query	Response
1	Sentence beginning “Our first example” OK as amended?	
2	We have separated and renumbered the two references in ref 15. Please check that subsequent renumbering is correct.	
3	Please check sentence beginning “One was”. I am not sure what you were referring to by “the other”. Do you mean the perovskite? Can we say “One was a Si_3N_4 glass similarly doped with Pt; the other, which adopted a lattice construct that was perfectly regular but randomized by atomic mixing, was a perovskite solid solution made into an epitaxial thin film to avoid line and planar defects that might have provided electrical shorts[17,18].”	
4	Changed to “application of a voltage” – OK?	
5	RF expanded OK?	
6	Changed to the proportional symbol – OK?	
7	There are no following sections – please check.	
8	Ref 9 – please check page range.	
9	What does the “c” represent in Fig 2b?	
10	Please check that the versions of Fig. 2 and 5a we have used are correct.	
11	Is there something missing after “100” here?	